

# Inferring the iron K emissivity profiles of accretion discs irradiated by extended coronae

Wenda Zhang (张文达)<sup>1,2\*</sup>, Michal Dovčiak<sup>2</sup>, Michal Bursa<sup>2</sup>, Jiří Svoboda<sup>2</sup>, Vladimír Karas<sup>2</sup>

<sup>1</sup>National Astronomical Observatories, Chinese Academy of Sciences, A20 Datun Road, Beijing 100101, China

<sup>2</sup>Astronomical Institute of the Czech Academy of Sciences, Boční II 1401, CZ-14100 Prague, Czech Republic

Accepted XXX. Received YYY; in original form ZZZ

## ABSTRACT

One of the most promising methods to measure the spin of an accreting black hole is fitting the broad iron  $K\alpha$  line in the X-ray spectrum. The line profile also depends on the geometry of the hard X-ray emitting corona. To put constraints on the black hole spin and corona geometry, it is essential to understand how do they affect the iron  $K\alpha$  line emissivity profile. In this work, we present calculations of the illumination and the iron  $K\alpha$  emissivity profiles performed with the Monte-Carlo GR radiative transfer code `MONK`. We focus on distinction between the illumination and emissivity profiles, which is in most previous studies neglected. We show that especially for the case of black hole X-ray binaries (BHXRBs), the difference is very large. For active galactic nuclei (AGNs), the emissivity profile has a more similar shape as the illumination profile, but it is notably steeper in the innermost region within a few gravitational radii. We find out that the different behavior between AGN and black hole X-ray binary discs is due to the different energy spectra of the illuminating radiation. This suggests that the emissivity profile of the iron  $K\alpha$  line cannot be determined by black hole spin and corona geometry alone and the energy spectrum of the illuminating radiation has to be taken into account. We also examined the effect of including the self-irradiation, and find it to be more important than the corona emission in BHXRBs.

**Key words:** methods: numerical — radiative transfer — relativistic processes — galaxies: active

## 1 INTRODUCTION

X-ray spectra of Active Galactic Nuclei (AGNs) and black hole X-ray binaries (BHXRBs) exhibit signatures of X-ray reflection, including the iron K fluorescent line and the Compton hump (see the review of Miller 2007). It is generally believed that they are due to the hard X-ray radiation of the corona illuminating the underlying accretion disc (see Fabian & Ross 2010, and references therein). The iron line is intrinsically narrow, but the observer at infinity sees a broad and asymmetric line profile, due to the gravitational redshift by the strong gravitational field of the black hole and due to the Doppler broadening (Fabian et al. 1989; Laor 1991). The shape of the broad iron line depends sensitively on the black hole spin, and thus fitting the iron line profile is one of the most promising methods of measuring the spin of accreting black holes in both XRBs (e.g. Blum et al. 2009; Miller et al. 2009, 2013; Parker et al. 2015; El-Batal et al. 2016; Miller et al. 2018; Xu et al. 2018a,b) and AGNs (e.g. Brenneman & Reynolds 2006; Miniutti et al. 2009a; Schmoll et al. 2009; Fabian et al. 2009; Brenneman et al. 2011; Emmanoulopoulos et al. 2011; Reynolds et al. 2012; Tan et al. 2012; Risaliti et al. 2013; Ricci et al. 2014; Agís-González et al. 2014; Sun et al. 2018; Jiang et al. 2019).

To put narrow constraints on black hole spins it is important to know the radial emissivity profile of the iron fluorescent line and to know how it depends on the black hole spin (Svoboda et al. 2012). Martocchia et al. (2000) and Miniutti et al. (2003) studied

the emissivity profile of an accretion disc illuminated by a point-like source above the disc and found the profile to be a three-segment broken power-law. Dovciak et al. (2014) investigated in detail the dependence of the emissivity profile on the black hole spin and corona height assuming the lamp-post geometry. Analysis of the emissivity profile of accretion discs irradiated by extended coronae was performed by Wilkins & Fabian (2012) and Gonzalez et al. (2017).

In most previous studies, the authors made no clear distinction between the illumination profile (the total energy of illuminating radiation per unit time per unit area) and the emissivity profile of a particular radiative process (the number of photons emitted per unit time per unit area). Also, simple assumptions were made for the spectrum of the illuminating radiation. For example, when calculating the iron  $K\alpha$  emissivity profile the spectrum was usually assumed to have a power-law shape in the energy band most relevant for iron K fluorescent lines. Unlike the illumination profile, the emissivity profile also depends on the specific radiative process and is thus sensitive to the local energy spectrum of the illuminating radiation. In this work, we present the illumination and iron  $K\alpha$  emissivity profiles obtained with a general relativistic (GR) Monte Carlo radiative transfer code `MONK` (Zhang et al. 2019). Thanks to its Monte Carlo nature we are able to calculate not only the flux but also the spectrum of the incoming illuminating radiation as measured in the rest frame of the disc fluid for accretion discs illuminated by extended coronae. As a result, we are able to calculate both the illumination and the corresponding emissivity profiles of each radius in the disc. Recently

\* wdzhang@nao.cas.cn

it has been shown that self-irradiation affects the reflection emission as well (e.g. Wilkins et al. 2020; Dauser et al. 2022). Therefore in this work, we also investigate the illumination and emissivity profiles of self-irradiation. While Wilkins et al. (2020); Dauser et al. (2022) studied the returning radiation of the reflection emission due to the coronal emission irradiating the disc, in this manuscript we are investigating the returning radiation of the thermal emission of the disc.

The paper is organized as follows. In Section 2 we illustrate the procedures of the numerical calculations. In Section 3 we present the results without taking into account the self-irradiation, while in Section 4 we present the results where self-irradiation is taken into consideration. The results are discussed in Section 5 and summarized in Section 6.

## 2 PROCEDURE

### 2.1 Calculating the illumination and emissivity profiles

We calculate the illumination and emissivity profiles of a razor-thin relativistic Keplerian disc illuminated by an extended corona. The thin disc extends down to the innermost stable circular orbit (ISCO). We assume that the thin disc follows the Novikov-Thorne effective temperature profile and there is zero torque at the inner boundary. We utilise the ‘‘superphoton’’ scheme in our simulation. In this scheme each superphoton is actually a photon package that consists of many photons with identical energy and momentum, and is assigned a statistical weight  $w$ . The weight  $w$  has the physical meaning of the number of photons generated per unit time as measured in a distant observer’s frame (for details, see Zhang et al. 2019). We sample seed superphotons from the thin disc and propagate the superphotons along null geodesics in the Kerr spacetime. Each superphoton is characterized by its energy at infinity  $E_\infty$ , weight  $w$ , initial position  $x_0^\mu$ , and initial wave vector  $k_0^\mu$ . If the superphoton is traveling inside the extended corona, we set the step of raytracing to be much less than the scattering mean free path. For each step, we evaluate the Compton scattering optical depth. If the superphoton is scattered, we sample the energy and momentum of the scattered superphoton assuming the Klein-Nishina differential cross-section. Finally, we collect superphotons that arrive back to the disc. For each superphoton, we have the following information:  $E_\infty$ ,  $w$ , and its position  $x^\mu$  and wave-vector  $k^\mu$  while hitting the disc.

The calculations are performed in the Boyer-Lindquist coordinate system with coordinates  $t, r, \theta, \phi$ . We divide the accretion disc into several radial bins, from the ISCO to  $100 \text{ GM}/c^2$ . The proper area of the  $i$ -th bin is

$$\begin{aligned} S_i &\equiv \int_0^{2\pi} \int_{r_i}^{r_{i+1}} \gamma \sqrt{g_{rr} g_{\phi\phi}} dr d\phi \\ &= \int_{r_i}^{r_{i+1}} \frac{2\pi \rho \gamma}{\sqrt{\Delta}} \sqrt{r^2 + a^2 + \frac{2a^2 r}{\rho^2}} dr \\ &= \int_{r_i}^{r_{i+1}} 2\pi u^t r dr d\phi, \end{aligned} \quad (1)$$

where  $\rho^2 \equiv r^2 + a^2 \cos^2 \theta$ ,  $\Delta \equiv r^2 - 2r + a^2$ ,  $\gamma$  is the Lorentzian factor of the disc fluid as measured by a stationary observer, and  $r_i, r_{i+1}$  are the lower and upper boundaries of the  $i$ -th radial bin, respectively, and  $u^t \equiv dt/d\tau$  is used to translate the time from a distant observer’s frame to the local frame:

$$u^t = \frac{1}{\sqrt{1 - 2/r + 4\Omega a/r - \Omega^2(r^2 + a^2 + 2a^2/r)}}, \quad (2)$$

where  $\Omega$  is the angular velocity of the disc fluid. In the  $i$ -th radial bin, the flux of the illuminating radiation in the unit of energy per unit time per unit area as measured by an observer co-rotating with the disc fluid is

$$\epsilon_i = \frac{\sum w E_{\text{disc}} u_i^t}{S_i}, \quad (3)$$

where the sum is over all Comptonized photons that strike the thin disc between  $r_i$  and  $r_{i+1}$ , and  $E_{\text{disc}}$  is the photon energy measured by the disc fluid. Denoting the four-velocity of the disc fluid  $U^\mu$ , we have  $E_{\text{disc}} = -k^\mu U_\mu E_\infty$ .

The probability for a hard X-ray photon to produce an iron  $K\alpha$  photon while striking the neutral disc is proportional to: (e.g. George & Fabian 1991):

$$P(E) \propto \frac{n_{\text{Fe}} \sigma_{\text{Fe}}(E)}{\sum n_j \sigma_{j,\text{abs}}(E) + n_e \sigma_{\text{sca}}(E)}, \quad (4)$$

if the energy of the hard X-ray photon is above the neutral iron K edge  $E_K$  ( $\sim 7.12 \text{ keV}$ ), where  $n_{\text{Fe}}$  is the number density of neutral iron,  $n_j$  is the number density of the  $j$ -th ion species,  $n_e$  is the number density of electrons,  $\sigma_{\text{Fe}}$  is the photon-ionization cross section of the neutral iron,  $\sigma_{j,\text{abs}}$  is the photon-ionization cross section of the  $j$ -th ion species, and  $\sigma_{\text{sca}}$  is the Compton scattering cross section. As  $\sigma_{\text{Fe}} \propto E^{-3}$  while  $\sigma_{\text{sca}}$  is varying slowly with energy,  $P(E)$  decreases with energy rapidly and the photons with energy just above the iron K edge are most essential for the production of iron  $K\alpha$  photons (George & Fabian 1991).

In the  $i$ -th radial bin, the emissivity of iron  $K\alpha$  photon, i.e. the number of iron  $K\alpha$  photons produced per unit area per unit time in the local frame is

$$\epsilon_i = \frac{\sum w P(E_{\text{disc}}) u_i^t}{S_i}, \quad (5)$$

where the sum is over all superphotons with  $r_i \leq r < r_{i+1}$  and  $E_{\text{disc}} \geq E_K$ .

In this paper, we assume that the elements in the disc atmosphere are neutral and have solar abundance (Grevesse & Sauval 1998). The photon ionization cross sections are calculated with analytical formulae by Verner & Yakovlev (1995). For Compton scattering we assume the Klein-Nishina scattering cross section.

### 2.2 Relation between the illumination and emissivity profiles

Let us assume that the spectra of the illuminating radiation at different radii on the disc differ only by different normalizations and redshift (which is the case for an isotropic, lamp-post corona). In this case, we can write the photon spectrum of the illuminating radiation as observed by the disc fluid located at radius  $r$  as

$$N(E, r) = F(r) f\left(\frac{E}{g(r)}\right) \frac{1}{g(r)}, \quad (6)$$

where  $F(r)$  is the radial distribution of the illuminating photons and is a function of  $r$  only,  $f(E)$  is the energy spectrum of the illuminating radiation in the rest frame of the corona, and  $g(r)$  is the redshift factor  $g \equiv E_{\text{disc}}/E_{\text{corona}}$ . Then the illuminating radiation profile is

$$\epsilon(r) = \int_0^{+\infty} EN(E, r) dE \propto F(r) g(r), \quad (7)$$

regardless of the spectral shape. The iron  $K\alpha$  emissivity profile

$$\epsilon(r) = \int_{E_K}^{\infty} N(E, r) P(E) dE = \frac{F(r)}{g(r)} \int_{E_K}^{\infty} P(E) f\left(\frac{E}{g(r)}\right) dE. \quad (8)$$

For Comptonized spectrum the high energy spectrum can usually be described by a cut-off power-law function  $f(E) = E^{-\Gamma} e^{-E/E_{\text{cut}}}$  for  $E \geq E_0$ , where  $\Gamma$  is the photon index,  $E_{\text{cut}}$  is the high-energy cut-off energy, and  $E_0$  is the energy of the low-energy cut-off. If  $E_0 \leq E_K / \max(g(r))$ , then

$$\varepsilon(r) = F(r) g^{\Gamma-1}(r) \int_{E_K}^{\infty} P(E) E^{-\Gamma} e^{-E/g(r)E_{\text{cut}}} dE. \quad (9)$$

For the iron  $K\alpha$  emissivity profile, as  $P(E)$  decrease rapidly with energy, the integral is not sensitive to  $g(r)$ , therefore

$$\varepsilon(r) \propto F(r) g^{\Gamma-1}(r), \quad (10)$$

and

$$\frac{\varepsilon(r)}{\varepsilon(r)} \propto g^{\Gamma-2}(r). \quad (11)$$

We can see that whether the emissivity profile is steeper than the illumination profile depends on the value of  $\Gamma$  and the shape of  $g(r)$ .

### 3 RESULTS

#### 3.1 Stationary spherical corona in AGNs

In this section, we present the illumination and emissivity profiles of accretion discs illuminated by a spherical corona above the disc. In the reminder of this paragraph we list the fiducial values of the simulations. The rapidly rotating ( $a = 0.998$ ) black hole with a mass of  $10^7 M_{\odot}$  is accreting with a mass accretion rate of  $4.32 \times 10^{23} \text{ g s}^{-1}$ . Assuming the radiative efficiency to be 0.354 for a spin 0.998 black hole, the bolometric luminosity is expected to be  $\sim 10\%$  the Eddington luminosity. The spherical corona is stationary, i.e. the fluid has the same angular velocity as a zero angular momentum observer. The temperature of the corona is 100 keV, and the Thomson optical depth of the corona  $\tau_T \equiv \sigma_T n_e R_c = 0.2$ , where  $\sigma_T$  is the Thomson scattering cross section, and  $R_c$  is the radius of the corona. Given  $\sigma_T$ , we immediately obtain the electron density of the corona. For each tiny step of raytracing, the procedure for evaluating the scattering optical depth can be found in Sec. 2.6.1 of [Zhang et al. \(2019\)](#).

##### 3.1.1 Dependence on the corona size

In Fig. 1, we present the illumination and emissivity profiles for spherical coronae of different sizes. The center of the corona is located on the black hole rotation axis,  $10 \text{ GM}/c^2$  above the equatorial plane. For all corona sizes the emissivity profile seems to be quite steep in the innermost region of the accretion disc (below  $\sim 2\text{--}3 \text{ GM}/c^2$ ), and becomes shallower as the radius increases. Then beyond  $\sim 10 \text{ GM}/c^2$ , it steepens again. We fit the emissivity profile in different regions on the accretion disc with a power-law model (i.e.  $\varepsilon(r) \propto r^{-q}$ ) using the least squared method, and summarize the results in Table 1. In the innermost region of the accretion disc ( $r \leq 2 \text{ GM}/c^2$ ), the emissivity profile becomes steeper as the corona radius decreases. Far away from the black hole ( $r \geq 20 \text{ GM}/c^2$ ), the indices are roughly consistent with the Newtonian value of 3. In the Newtonian case, for a lamp-post corona we expect illumination profile to have the following radial profile:

$$\varepsilon(r) \propto \frac{1}{(h^2 + r^2)^{3/2}}, \quad (12)$$

where  $h$  is the height of the corona, which has a power-law shape with an index of 3 at large radii and flattens in the inner region. This

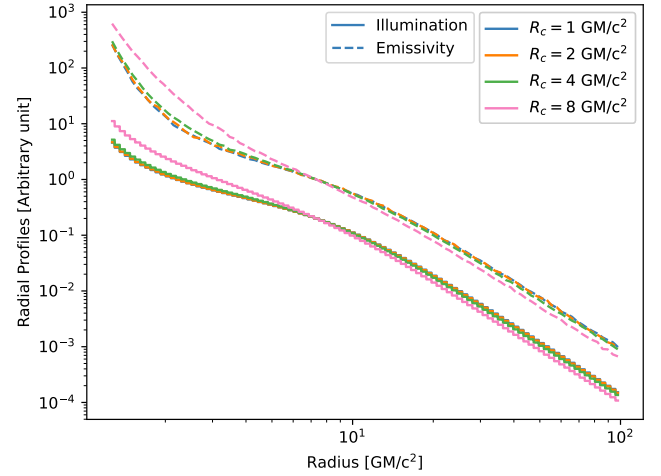


**Figure 1.** The illumination (solid lines) and emissivity (dashed lines) profiles of accretion discs illuminated by stationary spherical coronae of different sizes. Each corona is located on the symmetry axis of a  $10^7 M_{\odot}$  black hole,  $10 \text{ GM}/c^2$  above the equatorial plane.

**Table 1.** The fitted indices of the illumination and emissivity profiles, for accretion discs illuminated by spherical and slab coronae of various radii.

Geometry	$R_c$ [GM/c <sup>2</sup> ]	Illumination		Emissivity	
		$r < 2$	$r > 20$	$r < 2$	$r > 20$
Spherical	1	2.92	3.06	6.55	2.97
	2	2.92	3.06	6.49	3.00
	4	2.96	3.07	6.32	2.98
	8	3.27	3.09	5.67	3.02
Slab	1	2.84	3.06	6.09	2.95
	2	2.84	3.05	4.82	2.97
	4	2.92	3.08	4.42	3.00
	8	3.00	3.31	4.09	3.26

explains the radial profile in the intermediate and outer regions where the gravitational field is not profound. In the innermost region, the light-bending effect of the strong gravitational field leads to a steep profile.

The illumination profile has a similar three-segment broken power-law shape but in the innermost region it is shallower than the emissivity profile. We also fit the profiles and present the results in Table 1. We measure the photon index of the illuminating radiation in the energy band of 20–100 keV and find it to be  $\sim 3$ . According to [Dovciak et al. \(2014\)](#), in the innermost region of the accretion disc  $g(r)$  increases with decreasing radius. Therefore, the result that the emissivity profile is steeper than the illumination profile is consistent with Eq. 11.

##### 3.1.2 Dependence on the corona height

In Fig. 2, we present the illumination and emissivity profiles for spherical coronae located at different heights above the equatorial plane. The radius of the coronae is  $1 \text{ GM}/c^2$  for all cases. We fit the emissivity and illumination profiles in different regions and summarize the results in Table 2. In the innermost region, as the height increases, the emissivity profile becomes steeper. The illumination

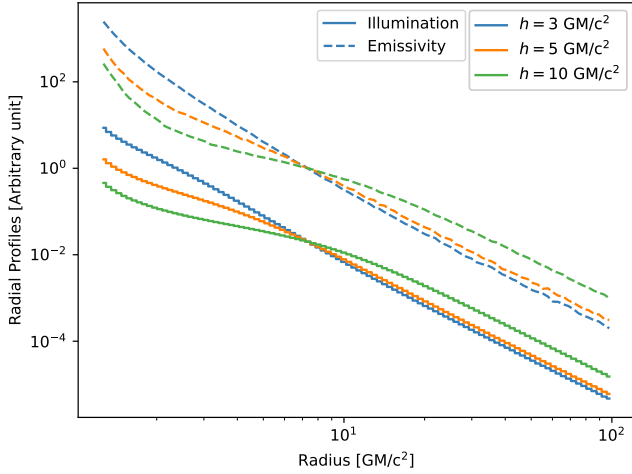


**Figure 2.** The same with Fig. 1, but for coronae with radius of  $1 \text{ GM}/c^2$  and various heights above the equatorial plane.

**Table 2.** The fitted indices of the illumination and emissivity profiles, for accretion discs illuminated by spherical and slab coronae of various heights in the lamp-post geometry.

Geometry	$h$ [ $\text{GM}/c^2$ ]	Illumination		Emissivity	
		$r < 2$	$r > 20$	$r < 2$	$r > 20$
Spherical	3	3.52	3.13	5.80	3.15
	5	3.01	3.12	5.90	3.13
	10	2.92	3.06	6.55	2.97
Slab, $R_c = 1 \text{ GM}/c^2$	3	2.30	3.19	4.72	3.28
	5	2.78	3.17	5.60	3.11
	10	2.84	3.06	6.09	2.95
Slab, $R_c = 8 \text{ GM}/c^2$	3	2.77	2.98	3.19	2.97
	5	3.15	3.02	3.74	3.02
	10	3.00	3.31	4.09	3.26

profile steepens towards lower height, which is similar with lamp-post corona (Dovciak et al. 2014), and is opposite to the emissivity profile.

### 3.1.3 Dependence on other parameters

We also investigate the effect of other, non-geometrical parameters of the corona on the illumination and emissivity profiles. We assume corona at a height of  $10 \text{ GM}/c^2$  and radius of  $1 \text{ GM}/c^2$ . We start with varying the optical depth of the corona while fixing other parameters at the fiducial values. In the top panel of Fig. 3, we present the profiles for various optical depths of the corona. The illumination profiles are identical for different optical depth, which is expected as the illumination profile is almost solely determined by the coronal geometry. In the innermost region, the emissivity profiles get shallower as the optical depth increases, consistent with our calculation in Sec. 2.2 (especially Eq. 11), as the photon index decreases with the optical depth. Similar analysis is done for the coronal temperature and the mass accretion rate, the results of which are shown in the middle and bottom panels of Fig. 3, respectively. Again, the illumination profile

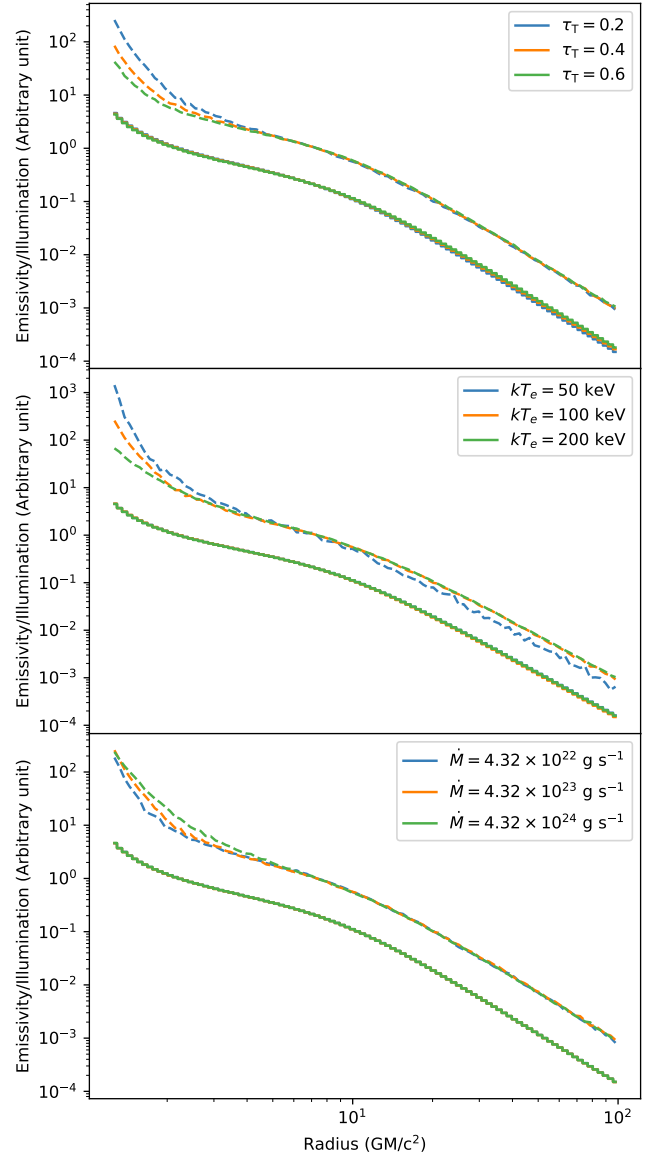


**Figure 3.** The illumination (solid) and emissivity (dashed) profiles of coronae with varying non-geometrical parameters. Top panel: the profiles of different optical depth of the corona. Middle: the profiles assuming various coronal temperature. Bottom: the profiles assuming various mass accretion rates of the disc.

is independent of these two parameters. The emissivity profile gets shallower with the increasing coronal temperature, due to the same reason with the dependence on the optical depth, that the spectrum hardens as the coronal temperature increases. The emissivity profile is also weakly dependent on the mass accretion rate, probably due to the mass accretion rate affecting the low-energy cut-off of the primary emission.

## 3.2 Co-rotating slab corona in AGNs

In this section, we present the results for accretion discs irradiated by slab coronae above the disc. The slab coronae are co-rotating with the underlying accretion disc. The thickness of the slab is  $2 \text{ GM}/c^2$ . The optical depth of the corona along the vertical direction is  $\tau_T \equiv$

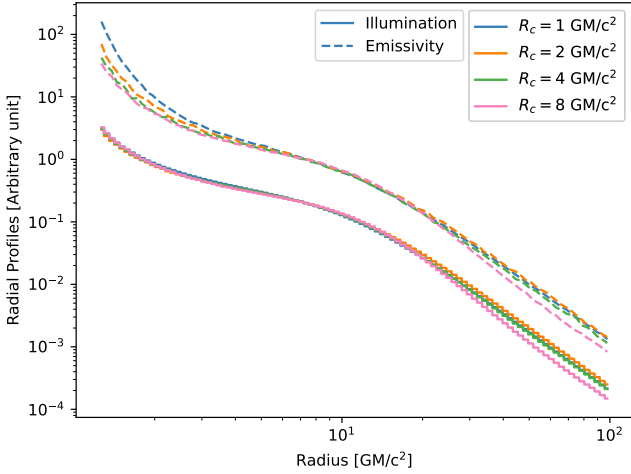


**Figure 4.** The illumination and emissivity profiles of accretion discs illuminated by co-rotating slab coronae of different sizes. The coronae have a thickness of  $2 \text{ GM}/c^2$  and are located on the symmetry axis of a  $10^7 M_\odot$  black hole,  $10 \text{ GM}/c^2$  above the equatorial plane. The various radial extents of the slab coronae along the horizontal direction are indicated in the figure.

$n_e \sigma_T h_c / 2 = 0.2$ , where  $h_c$  is the thickness of the corona, and the temperature of the corona is  $100 \text{ keV}$ . The black hole and thin disc have the same properties as in the previous subsection.

### 3.2.1 Dependence on the corona size

In Fig. 4, we present the illumination and emissivity profiles for accretion discs irradiated by slab coronae of different sizes. Compared with the spherical coronae, the emissivity profile is more sensitive to the corona size, with shallower emissivity from more extended corona. Similarly with spherical coronae, the illumination profile is shallower than the emissivity profile given the same corona size. We fit the profiles and tabulate the results in Table 1.

### 3.2.2 Dependence on the corona height

In Fig. 5, we present the illumination and emissivity profiles for accretion discs irradiated by slab coronae located at different heights above the accretion disc. As the height increases, both the emissivity and the illumination profiles become steeper in the innermost region. The fitting results are tabulated in Table 2.

## 3.3 Stationary spherical coronae in BHXRBs

In Fig. 6, we present the illumination and emissivity profiles of accretion discs in BHXRBs illuminated by spherical coronae. The parameters are the same as for AGNs in Section 3.1, but for a  $M = 10 M_\odot$  black hole accreting at a rate of  $4.32 \times 10^{17} \text{ g s}^{-1}$  (corresponding to 10% Eddington luminosity). The emissivity profile is distinct compared with the emissivity profile of AGNs (Fig. 1) in that the profile is shallower than the Newtonian case below  $\sim 10 \text{ GM}/c^2$ , and the emissivity even decreases towards lower radius below  $\sim 1.6 \text{ GM}/c^2$ .

To highlight the distinction in the emissivity profile, in the upper panel of Fig. 7 we compare the profiles of accretion discs around  $10 M_\odot$  and  $10^7 M_\odot$  black holes. The illumination profiles are almost identical while the difference in the iron  $K\alpha$  emissivity profile is

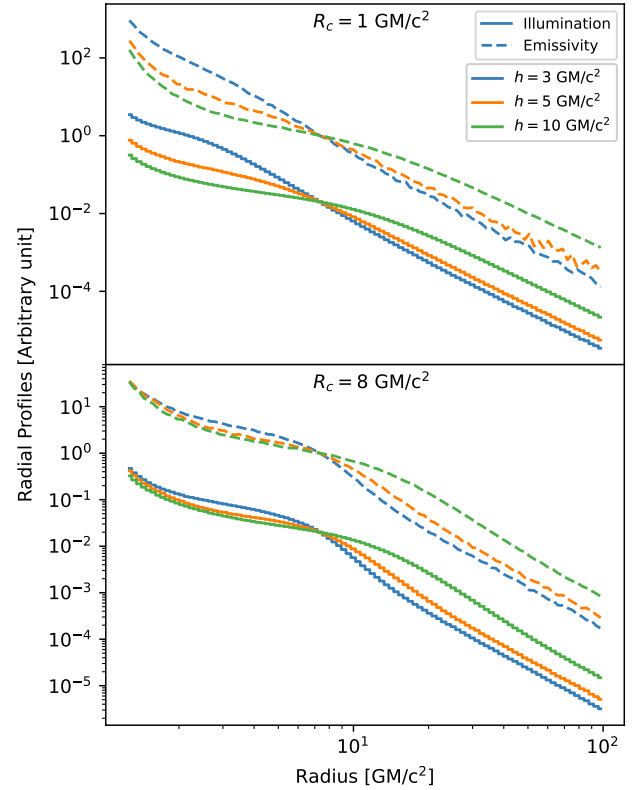


**Figure 5.** The same with Fig. 4, but for coronae with the same radial extent but various heights above the accretion discs. In the upper and lower panels we present the profiles for corona radii of 1 and  $8 \text{ GM}/c^2$ , respectively.

obvious. An immediate consequence is that the iron line profile becomes different. We calculate the iron line profile seen by an observer at an inclination of  $60^\circ$ , assuming isotropic iron line emission in the rest frame of the disc. The results are presented in the lower panel of Fig. 7. Assuming the same corona geometry, the iron line profiles from AGNs and XRB are clearly different, with the latter weaker in the red wing.

To find out the reason that causes the difference, we calculate the spectra of the illuminating radiation as observed by the disc fluid at radii of  $1.27$ ,  $1.58$ , and  $2.67 \text{ GM}/c^2$ , respectively, and present the results in Fig. 8. The spectra can be described as a broken power-law with a low-energy spectral break roughly at the temperature of the seed photon. While the break energy should stay the same in the rest frame of the corona, the change of the redshift factor across the accretion disc results in different break energies of the illuminating radiation. For  $M = 10^7 M_\odot$ , the break energy is always lower than  $E_K$ . In this case, a higher redshift simply leads to more X-ray photons above  $E_K$ ; whereas for the  $10 M_\odot$  case, the break energy of the photon spectra is in the range of  $2 - 10 \text{ keV}$ , resulting in a distinct emissivity profile. This indicates that the energy spectra of the hard X-ray radiation could substantially affect the emissivity profile.

In the most popular scenario of the spectral states of BHXRBs, the standard disc during the hard spectral state is truncated at a radius larger than the ISCO (e.g. Esin et al. 1997). We therefore perform simulations to assess the illumination and emissivity profiles for truncated discs. In Fig. 9 we present the profiles for discs truncated at radii of  $10$  (blue) and  $20 \text{ GM}/c^2$  (orange), and compare the results

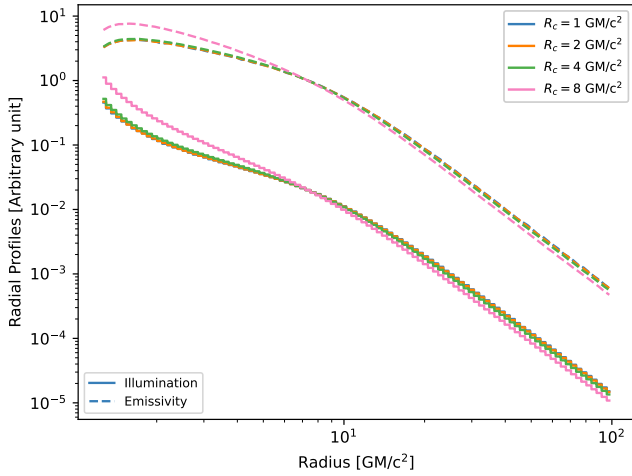


**Figure 6.** The same with Fig. 1, but for a  $10 M_{\odot}$  black hole.

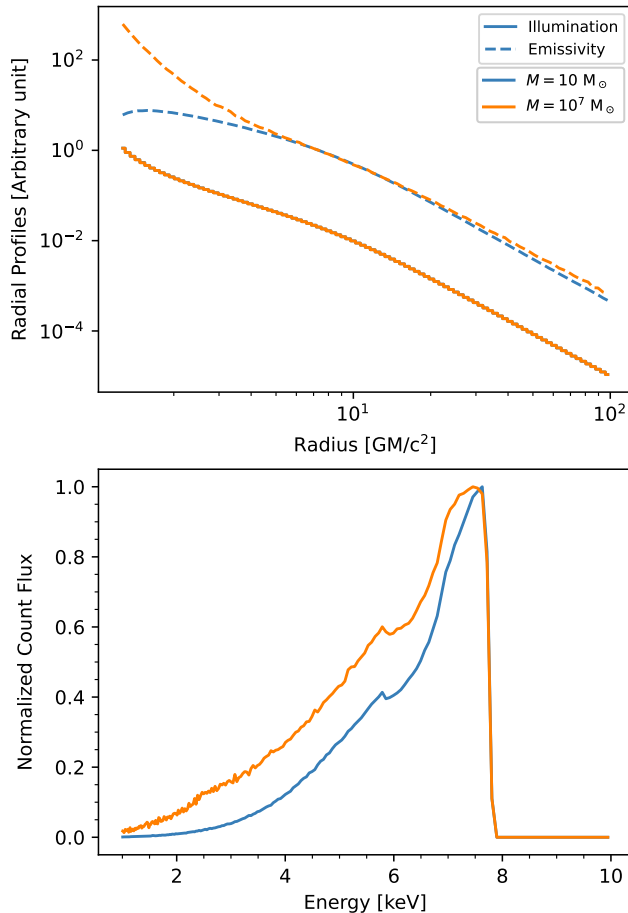


**Figure 7.** The upper panel: a comparison between the emissivity (dashed) and illumination profiles of accretion discs in a BHXRB (blue) and in an AGN (orange). In both cases the accretion discs are illuminated by a stationary spherical corona with a height of  $10 \text{ GM}/c^2$  and a radius of  $1 \text{ GM}/c^2$ . The lower panel: the line profiles corresponding to the emissivity profiles in the upper panel, for an observer at an inclination of  $60^\circ$ .

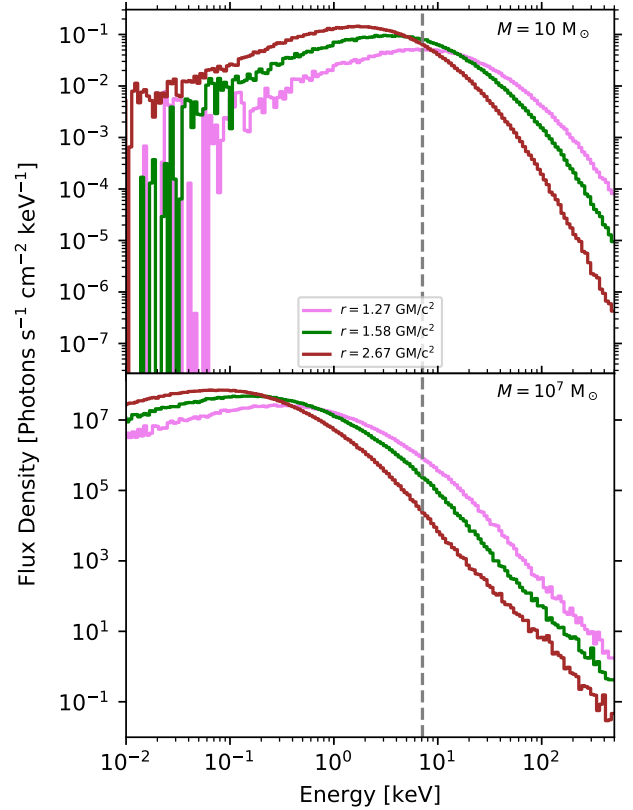


**Figure 8.** The energy spectra of the illuminating radiation observed by disc fluid located at different radii. The spherical corona is located  $10 \text{ GM}/c^2$  above the accretion disc and has radius of  $1 \text{ GM}/c^2$ . The spectra at different radii are plotted in different colors. The vertical dashed line indicates the location of neutral iron K edge at  $7.12 \text{ keV}$ . In the upper and lower panels we present the spectra for accretion discs around black holes with masses of  $10$  and  $10^7 M_{\odot}$ , respectively.

with discs truncated at the ISCO (black). Beyond the truncation radius, the illumination and emissivity profiles of truncated disc seem to be almost the same with the profiles of accretion discs truncated at ISCO, indicating that the profiles are rather insensitive to the truncation radius.

#### 4 THE EFFECT OF SELF-IRRADIATION

So far we have considered the irradiation of the corona emission only. In fact, due to the light-bending effect of the strong gravitational field in the vicinity the black hole, the accretion disc, especially the inner part of it, is also irradiated by photons from the opposite side of the disc, which is commonly referred to as self-irradiation. In this section we investigate the illumination and emissivity profile after taking the self-irradiation into account. The calculations are done utilizing equations 3 and 5, in a similar fashion with the corona radiation, except that the sum is now over all the self-irradiating photons.

##### 4.1 BHXRB

In Fig. 10, we present the illumination and emissivity profiles of the self-irradiation in a BHXRB and compare them with the profiles of

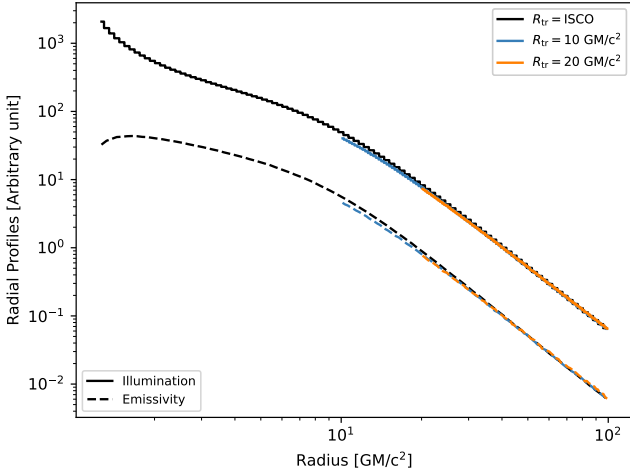


**Figure 9.** The same with Fig. 6, but for various truncation radii  $R_{\text{tr}}$ , as indicated in the plot.

the corona emission. For a compact corona with radius of  $1 \text{ GM}/c^2$  (the upper panel), the illumination is dominated by self-irradiation, while the corona emission is weaker by  $\sim 2$  orders of magnitudes. In contrast with the three-segment-power-law shape of the illumination profile of the corona emission, the illumination profile of the self-irradiation seems to have a power-law shape without obvious breaks. The iron  $K\alpha$  emissivity profile also has a power-law shape down to the innermost region of the accretion disc. The profiles for a more extended corona ( $R_c = 8 \text{ GM}/c^2$ ) are plotted in the lower panel of Fig. 10. The illumination from the corona and the self-irradiation are comparable beyond  $\sim 10 \text{ GM}/c^2$ , whilst in the inner region the self-irradiation is more important. We would also expect the relative importance of the self-irradiation to be smaller if the disc is truncated, as the self-irradiation is due to the strong gravitational field close to the black hole.

In Fig. 11, we present the energy spectra of the corona emission and self-irradiation as seen by disc fluid located at a radius of  $2.67 \text{ GM}/c^2$ . For corona radius of  $1 \text{ GM}/c^2$  (the upper panel), the self-irradiation is brighter than the corona emission below  $\sim 30 \text{ keV}$ . As the corona becomes more extended with a radius of  $8 \text{ GM}/c^2$  (the lower panel), the self-irradiation barely changes but the corona emission becomes much stronger, therefore the critical energy below which the self-irradiation dominates drops to  $\sim 15 \text{ keV}$ , lower than the case of  $R_c = 1 \text{ GM}/c^2$ , but still above the iron K edge. Therefore, we expect that in BHXRBS the self-irradiation plays an important role in the iron K emission process. This is demonstrated in Fig. 12, in which the energy spectra of the iron K line are presented.

## 4.2 AGNs

In Fig. 13, we plot the spectra of self-irradiation in AGNs. The behavior of the illumination profile is the same with the BHXRBS case. In contrast, the self-irradiation is barely contributing to the production of the iron K line, and the iron K emissivity is dominated by the corona emission. The reason is that the cooler self-irradiation in AGNs cannot reach the iron K edge. This can be clearly seen in Fig. 14, where we present the energy spectra of the corona emission as well as self-irradiation. The  $\nu F_\nu$  spectrum of self-irradiation is peaked at  $\sim 0.2 \text{ keV}$  and its contribution disappear above  $\sim 1 \text{ keV}$ . In contrast with the iron  $K\alpha$  emission, the soft excess component in

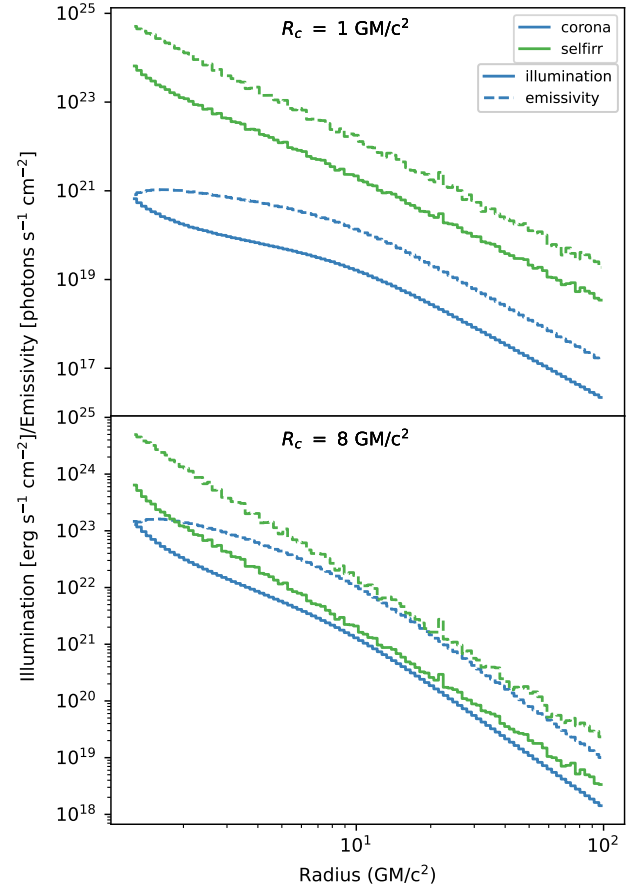


**Figure 10.** The illumination and iron  $K\alpha$  emissivity profiles of the corona emission in blue and of the self-irradiation in cyan, for a BHXRBS with a black hole mass of  $10 M_\odot$ . Note that here the profiles are in physical units. The profiles for coronae with radii of 1 and  $8 \text{ GM}/c^2$  are presented in the upper and lower panels, respectively.

the reflection spectrum would be affected by the self-irradiation, as discussed in more details in Section 5.2.

## 5 DISCUSSION

### 5.1 A summary of our results

The trajectory of a photon in vacuum is independent of the energy of the photon. As a result, given two disc-corona systems with the same black hole spin and geometries (in geometrical units) but with different mass, we would expect nearly the same radial distribution of the Comptonized photons that strike the underlying disc, independent of the mass of the black hole.

However, the reflection emission depends not only on the flux but also on the spectral shape of the illuminating coronal emission. One example is the iron  $K\alpha$  line in the reflection spectrum (see equation 4). The energy spectrum of the corona radiation as seen by the disc depends on the temperature of the disc, which is sensitive to the mass of the black hole and the mass accretion rate. This is demonstrated in Section 3, where we show that the discs in AGNs and XRBS have identical illumination profiles but distinct iron  $K\alpha$  emissivity profiles.

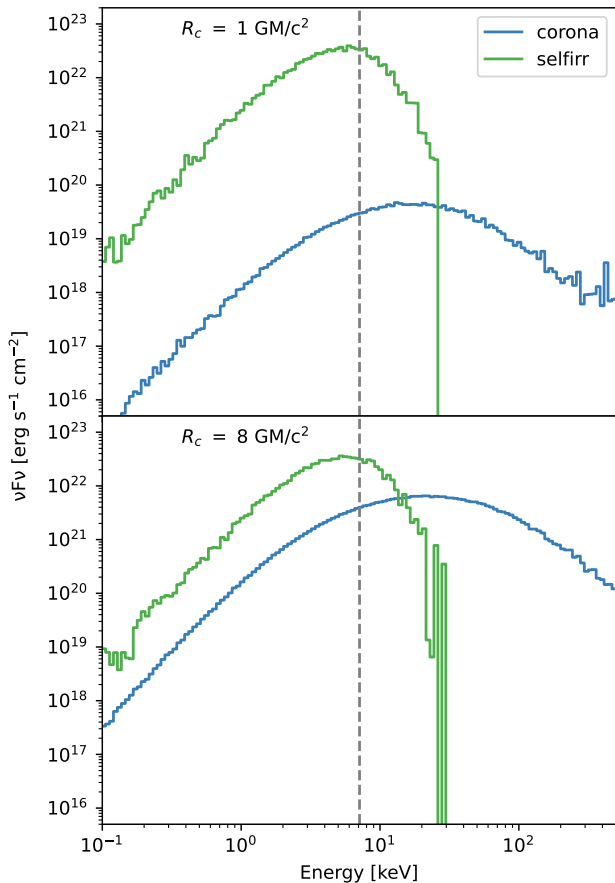


**Figure 11.** The energy spectra of the corona emission (blue) and the self-irradiation (cyan), as seen by the disc fluid located at a radius of  $2.67 \text{ GM}/c^2$ , for a BHXRBB with a black hole mass of  $10 M_{\odot}$ . The spectra for corona radii of 1 and  $8 \text{ GM}/c^2$  are plotted in the upper and lower panels, respectively. In both panels, the energy of the iron K edge at  $7.12 \text{ keV}$  is indicated by a vertical dashed line.

We note that we make simple assumptions on the corona and the disc. For instance, we assume a razor-thin disc, while in reality the disc should have finite thickness (e.g. Taylor & Reynolds 2018). We also assume spherical or slab coronae, in contrast to vertically extended corona that are studied in a few works (e.g. Chainakun & Young 2017; Lucchini et al. 2023). A more formal treatment of the reflection spectrum should also take into account the physical properties, e.g. the density of the disc (e.g. Jiang et al. 2022). While in future works we are going to investigate disc and corona with more realistic assumptions, we emphasize that the difference in the illumination and emissivity profiles we find in this work is more related with the fact that we consider the energy spectrum of the primary emission as received by the disc, and therefore we would tentatively expect that this effect is less sensitive to the geometrical parameters of the disc or the corona and the density of the disc.

## 5.2 Self-irradiation and the soft excess

Below  $\sim 1 - 2 \text{ keV}$ , the soft X-ray spectra of many AGNs exhibit excess with respect to the power-law continuum, known as “soft excess”. This feature was first noticed by Arnaud et al. (1985) and Singh et al. (1985), and later found in many Seyfert galaxies (e.g.

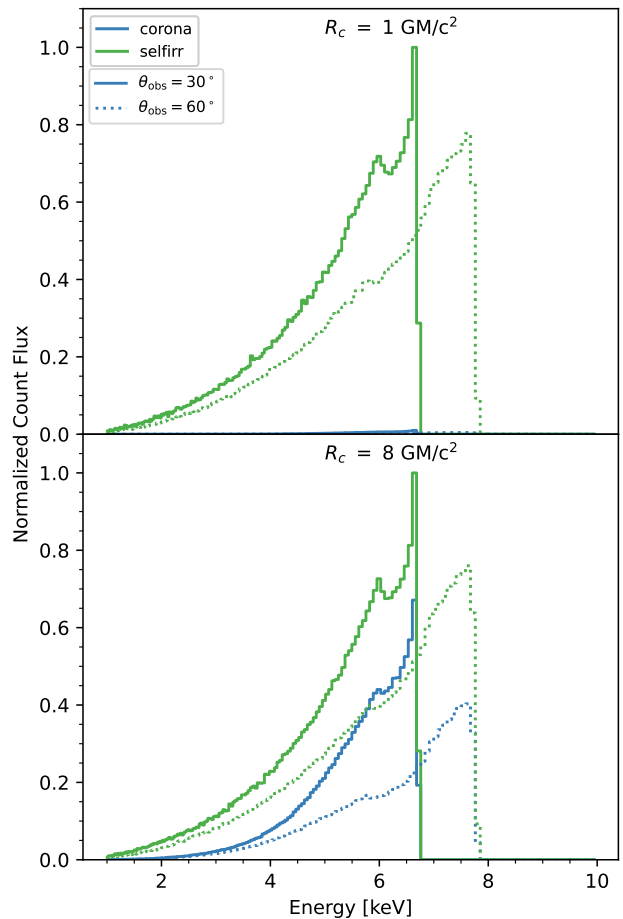


**Figure 12.** The profiles of the iron line as observed by observers at inclinations of  $30^\circ$  (solid lines) and  $60^\circ$  (dashed lines), corresponding to the emissivity profiles in Fig. 10. The contributions of the corona and self-irradiation are plotted in blue and cyan colors, respectively. The results for corona radii of 1 and  $8 \text{ GM}/c^2$  are plotted in the upper and lower panels, respectively.

Pounds et al. 1986; Turner & Pounds 1988; Walter & Fink 1993; Page et al. 2004; Porquet et al. 2004; Crummy et al. 2006; Bianchi et al. 2009; Miniutti et al. 2009b).

Currently there are two most popular explanations for the soft excess in AGNs: warm corona and ionized reflection. In the warm corona scenario, the soft excess is due to a “warm” corona Compton up-scattering optical/UV photons originating from the underlying thin disc (e.g. Czerny & Elvis 1987; Magdziarz et al. 1998; Done et al. 2012; Petrucci et al. 2013, 2018; Middei et al. 2019). Compared with the hot corona that is responsible for the hard X-ray continuum emission, the warm corona has larger optical depth  $\sim 10 - 20$  and lower temperature. On the other hand, the ionized reflection model could equally fit the energy spectrum of the soft excess (e.g. Balantyne et al. 2001; Fabian et al. 2002; Crummy et al. 2006). In this scenario, the soft X-ray emission lines in the reflection spectrum are emerging close to the black hole, and are thus greatly blurred by the strong gravitational field, leading to the soft excess. One argument against the reflection scenario is that the strength of the soft excess component is uncorrelated with the reflection strength (Boissay et al. 2016).

In Fig. 14, we see that for compact coronae with radius  $\lesssim 4 \text{ GM}/c^2$ , below  $\sim 1 \text{ keV}$  the self-irradiation is a dominating source in interact-

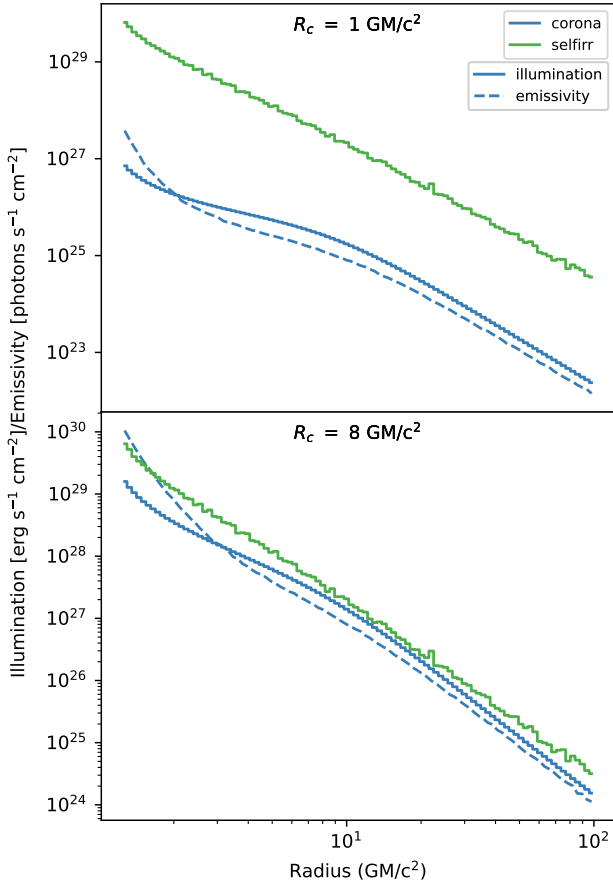


**Figure 13.** The same with Fig. 10, but for an AGN with black hole mass of  $10^7 M_{\odot}$ . The self-irradiation is barely contributing to the iron line emissivity.

ing with the disc atmosphere. By analyzing simultaneous UV/optical spectra of a subsample of CHEESE, we found that most of the AGNs in the subsample have corona radius smaller than  $4 \text{ GM}/c^2$  if assuming the height of the corona to be  $10 \text{ GM}/c^2$  (Ursini et al. 2020). Therefore, the self-irradiation is more relevant than the hot corona emission for the reflection features in the soft X-ray band, including the soft excess. However, this component has not been addressed in earlier works. On the other hand, given the energy of the high-energy cutoff of the self-irradiation component, the self-irradiation has negligible effect on the reflection continuum or the iron  $K\alpha$  line. Therefore, we do not expect the strength of the soft excess to be correlated with the strength of the reflection emission.

### 5.3 Anisotropic corona emission

In Zhang et al. (2019), we studied the angular dependence of Comptonized radiation. We found that for disc-corona systems in AGNs, the observer at lower inclination sees harder and less luminous Comptonized radiation, due to anisotropic seed photons. To assess the effect on the reflection spectrum, in Zhang et al. (2019) we considered an ideal case where a spherical plasma cloud Comptonizes low-frequency unidirectional seed photons. We found that the Comptonized radiation with inclination greater than  $90^\circ$ , which is an analog to corona emission that reaches the accretion disc, is more luminous than the Comptonized radiation with inclination less than  $90^\circ$ .

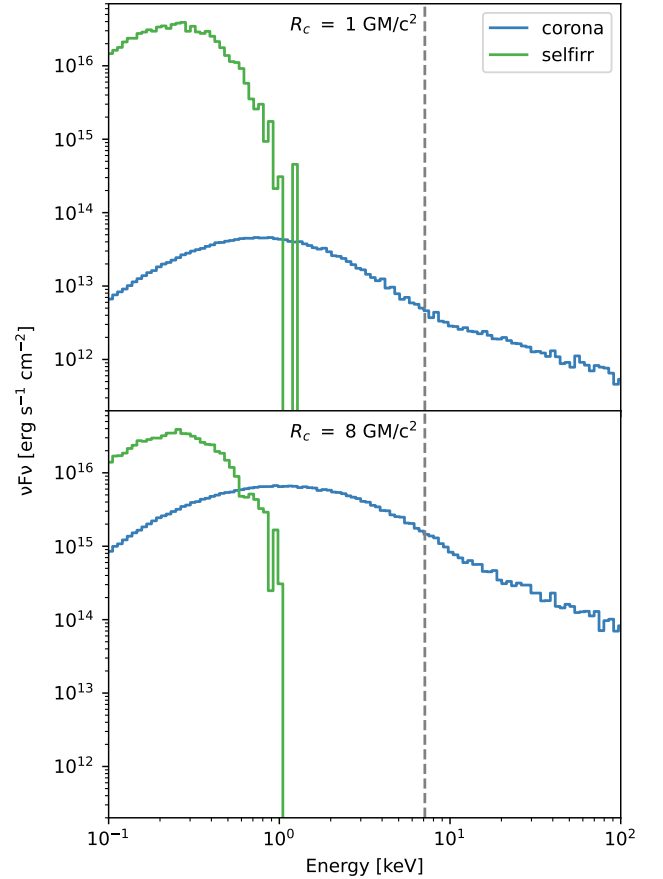


**Figure 14.** The same with Fig. 11, but for an AGN with a black hole mass of  $10^7 M_{\odot}$ .

Here, we calculate the angular dependent Comptonized spectra in *the rest frame of the extended corona*. We perform the calculation for compact spherical coronae (with radii of  $1 \text{ GM}/c^2$ ), for which we can safely assume that the lensing and redshift properties of the corona emission is close to a lamp-post corona at the same height. To assess these two effects, we sample  $N_{\text{tot}}$  photons originating from an isotropic lamp-post corona, and count the number of photons that reach an inclination bin at infinity or a ring on the accretion disc. The solid angle subtended by the inclination bin or the ring  $d\Omega = 4\pi N/N_{\text{tot}}$ , where  $N$  is the number of photons that falling into the inclination bin or the ring. Having known  $d\Omega$  and  $g$ , the spectral luminosity in the corona rest frame is

$$L_E = \frac{4\pi \sum_i w_i E_{i,\infty} / g_i}{d\Omega \Delta E}, \quad (13)$$

where the sum is over all superphotons with energy between  $E - \Delta E/2$  and  $E + \Delta E/2$ .

The spectra are presented in Fig. 15, for corona heights of 3, 10, and  $20 \text{ GM}/c^2$ , respectively. The dependence of the spectra on the inclination is similar with what we found in Zhang et al. (2019). This demonstrates our conclusion in Zhang et al. (2019) that the Comptonized radiation irradiating the disc is less luminous and harder than that reaching infinity, as the radius decreases. The spectra are also more anisotropic as the height increases, as the seed photons are getting more anisotropic.

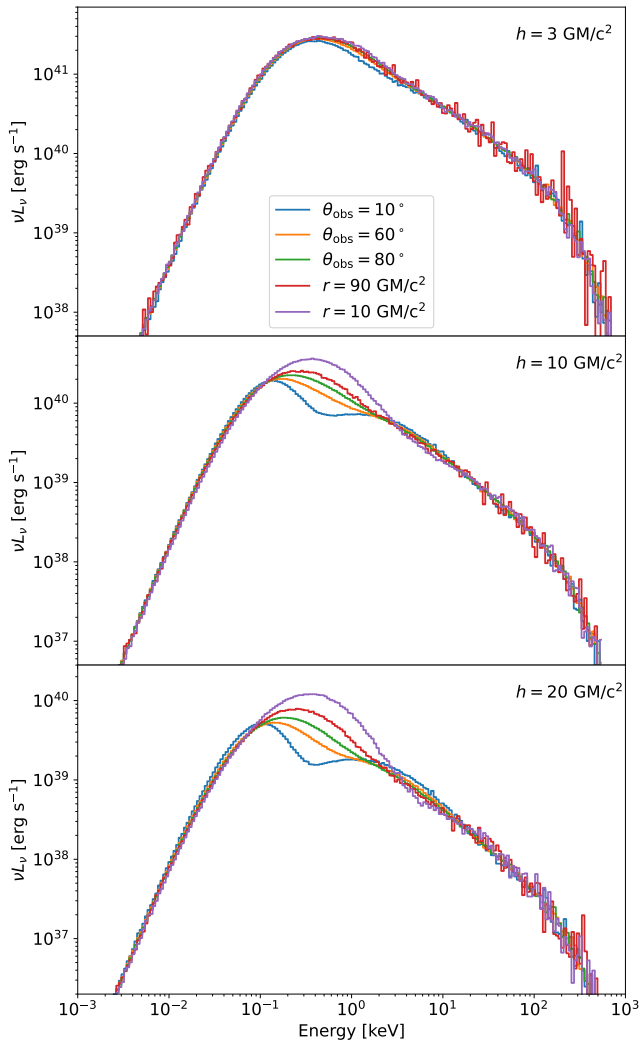


**Figure 15.** The energy spectra of the Comptonized emission, as seen by observers at various inclinations and by observers located at different radii on the accretion disc. The results for coronal heights of 3, 10, and 20  $\text{GM}/c^2$  are plotted in the top, middle, and bottom panels, respectively.

## 6 SUMMARY

In this work, we present the illumination and neutral iron  $K\alpha$  emissivity profiles of accretion discs irradiated by extended coroneae in simple spherical, lamp-post, and slab geometry. With our GR Monte Carlo radiative transfer code `MONK`, we calculated the energy spectrum of the illuminating radiation in the rest frame of the accretion disc. As a result, we are able to calculate both the illumination and emissivity profiles while in most previous studies the authors did not make a clear distinction between the two. For AGN discs, the emissivity profiles are in general steeper than the illumination profiles for the parameters taken in the calculations; whereas for accretion discs in black hole X-ray binaries, the distinction is more dramatic: the emissivity even decreases with decreasing radius in the innermost region of the disc. We find out that the different behavior in AGNs and black hole X-ray binaries are due to the difference in energy spectra of the illuminating radiation as seen by the disc. This suggests that the emissivity profile of the iron  $K\alpha$  line cannot be determined by black hole spin and corona geometry alone, but the energy spec-

trum of the illuminating radiation has to be taken into account. We study the dependence of the emissivity profile on the geometry of the corona and find the emissivity in the innermost region of the disc steepens as the corona becomes less extended or as the corona has a larger height.

We also examine the effect of the self-irradiation. We find that for BHXRBs, the self-irradiation might be more important than the corona emission for the production of iron  $K\alpha$  emission, especially when the corona has large extension and when the inner edge of the disc is close to the black hole. The self-irradiation in AGNs has lower temperature than the iron K edge, therefore having no effect on the iron K emission. However, the self-irradiation may be important for the soft excess component.

## ACKNOWLEDGEMENTS

We thank the anonymous referee for his/her useful comments that greatly improved the manuscript. WZ acknowledges the support by the Strategic Pioneer Program on Space Science, Chinese Academy of Sciences through grants XDA15310000, and the support by the Strategic Priority Research Program of the Chinese Academy of Sciences, Grant No. XDB0550200. This work is also supported by the National Natural Science Foundation of China (grant 12333004). MD, MB, VK, and JS thank for the support from the GACR project 21-06825X and the institutional support from RVO:67985815. This research makes uses of `MATPLOTLIB` (Hunter 2007), a Python 2D plotting library which produces publication quality figures.

## DATA AVAILABILITY

The authors agree to make simulation data supporting the results in this paper available upon reasonable request.

## REFERENCES

- Agís-González, B., Miniutti, G., Kara, E., et al. 2014, *MNRAS*, 443, 2862, doi: [10.1093/mnras/stu1358](https://doi.org/10.1093/mnras/stu1358)
- Arnaud, K. A., Branduardi-Raymont, G., Culhane, J. L., et al. 1985, *MNRAS*, 217, 105, doi: [10.1093/mnras/217.1.105](https://doi.org/10.1093/mnras/217.1.105)
- Ballantyne, D. R., Iwasawa, K., & Fabian, A. C. 2001, *MNRAS*, 323, 506, doi: [10.1046/j.1365-8711.2001.04234.x](https://doi.org/10.1046/j.1365-8711.2001.04234.x)
- Bianchi, S., Guainazzi, M., Matt, G., Fonseca Bonilla, N., & Ponti, G. 2009, *A&A*, 495, 421, doi: [10.1051/0004-6361/200810620](https://doi.org/10.1051/0004-6361/200810620)
- Blum, J. L., Miller, J. M., Fabian, A. C., et al. 2009, *ApJ*, 706, 60, doi: [10.1088/0004-637X/706/1/60](https://doi.org/10.1088/0004-637X/706/1/60)
- Boissay, R., Ricci, C., & Paltani, S. 2016, *A&A*, 588, A70, doi: [10.1051/0004-6361/201526982](https://doi.org/10.1051/0004-6361/201526982)
- Brenneman, L. W., & Reynolds, C. S. 2006, *ApJ*, 652, 1028, doi: [10.1086/508146](https://doi.org/10.1086/508146)
- Brenneman, L. W., Reynolds, C. S., Nowak, M. A., et al. 2011, *ApJ*, 736, 103, doi: [10.1088/0004-637X/736/2/103](https://doi.org/10.1088/0004-637X/736/2/103)
- Chainakun, P., & Young, A. J. 2017, *MNRAS*, 465, 3965, doi: [10.1093/mnras/stw2964](https://doi.org/10.1093/mnras/stw2964)
- Crummy, J., Fabian, A. C., Gallo, L., & Ross, R. R. 2006, *MNRAS*, 365, 1067, doi: [10.1111/j.1365-2966.2005.09844.x](https://doi.org/10.1111/j.1365-2966.2005.09844.x)
- Czerny, B., & Elvis, M. 1987, *ApJ*, 321, 305, doi: [10.1086/165630](https://doi.org/10.1086/165630)
- Dauser, T., García, J. A., Joyce, A., et al. 2022, *MNRAS*, 514, 3965, doi: [10.1093/mnras/stac1593](https://doi.org/10.1093/mnras/stac1593)
- Done, C., Davis, S. W., Jin, C., Blaes, O., & Ward, M. 2012, *MNRAS*, 420, 1848, doi: [10.1111/j.1365-2966.2011.19779.x](https://doi.org/10.1111/j.1365-2966.2011.19779.x)
- Dovciak, M., Svoboda, J., Goosmann, R. W., et al. 2014, arXiv:1412.8627, <http://asc1.net/1412.8627>

- El-Batal, A. M., Miller, J. M., Reynolds, M. T., et al. 2016, *ApJL*, 826, L12, doi: [10.3847/2041-8205/826/1/L12](https://doi.org/10.3847/2041-8205/826/1/L12)
- Emmanoulopoulos, D., Papadakis, I. E., McHardy, I. M., et al. 2011, *MNRAS*, 415, 1895, doi: [10.1111/j.1365-2966.2011.18834.x](https://doi.org/10.1111/j.1365-2966.2011.18834.x)
- Esin, A. A., McClintock, J. E., & Narayan, R. 1997, *ApJ*, 489, 865
- Fabian, A. C., Ballantyne, D. R., Merloni, A., et al. 2002, *MNRAS*, 331, L35, doi: [10.1046/j.1365-8711.2002.05419.x](https://doi.org/10.1046/j.1365-8711.2002.05419.x)
- Fabian, A. C., Rees, M. J., Stella, L., & White, N. E. 1989, *MNRAS*, 238, 729
- Fabian, A. C., & Ross, R. R. 2010, *Space Science Reviews*, 157, 167, doi: [10.1007/s11214-010-9699-y](https://doi.org/10.1007/s11214-010-9699-y)
- Fabian, A. C., Zoghbi, A., Ross, R. R., et al. 2009, *Nature*, 459, 540, doi: [10.1038/nature08007](https://doi.org/10.1038/nature08007)
- George, I. M., & Fabian, A. C. 1991, *MNRAS*, 249, 352, doi: [10.1093/mnras/249.2.352](https://doi.org/10.1093/mnras/249.2.352)
- Gonzalez, A. G., Wilkins, D. R., & Gallo, L. C. 2017, *MNRAS*, 472, 1932, doi: [10.1093/mnras/stx2080](https://doi.org/10.1093/mnras/stx2080)
- Grevesse, N., & Sauval, A. J. 1998, *Space Science Reviews*, 85, 161, doi: [10.1023/A:1005161325181](https://doi.org/10.1023/A:1005161325181)
- Hunter, J. D. 2007, *Computing in Science Engineering*, 9, 90, doi: [10.1109/MCSE.2007.55](https://doi.org/10.1109/MCSE.2007.55)
- Jiang, J., Dauser, T., Fabian, A. C., et al. 2022, *MNRAS*, 514, 1107, doi: [10.1093/mnras/stac1144](https://doi.org/10.1093/mnras/stac1144)
- Jiang, J., Walton, D. J., Fabian, A. C., & Parker, M. L. 2019, *MNRAS*, 483, 2958, doi: [10.1093/mnras/sty3228](https://doi.org/10.1093/mnras/sty3228)
- Laor, A. 1991, *ApJ*, 376, 90, doi: [10.1086/170257](https://doi.org/10.1086/170257)
- Lucchini, M., Mastroserio, G., Wang, J., et al. 2023, *ApJ*, 951, 19, doi: [10.3847/1538-4357/acd24f](https://doi.org/10.3847/1538-4357/acd24f)
- Magdziarz, P., Blaes, O. M., Zdziarski, A. A., Johnson, W. N., & Smith, D. A. 1998, *MNRAS*, 301, 179, doi: [10.1046/j.1365-8711.1998.02015.x](https://doi.org/10.1046/j.1365-8711.1998.02015.x)
- Martocchia, A., Karas, V., & Matt, G. 2000, *MNRAS*, 312, 817, doi: [10.1046/j.1365-8711.2000.03205.x](https://doi.org/10.1046/j.1365-8711.2000.03205.x)
- Middei, R., Bianchi, S., Petrucci, P.-O., et al. 2019, *MNRAS*, 483, 4695, doi: [10.1093/mnras/sty3379](https://doi.org/10.1093/mnras/sty3379)
- Miller, J. M. 2007, *ARA&A*, 45, 441, doi: [10.1146/annurev.astro.45.051806.110555](https://doi.org/10.1146/annurev.astro.45.051806.110555)
- Miller, J. M., Reynolds, C. S., Fabian, A. C., Miniutti, G., & Gallo, L. C. 2009, *ApJ*, 697, 900, doi: [10.1088/0004-637X/697/1/900](https://doi.org/10.1088/0004-637X/697/1/900)
- Miller, J. M., Parker, M. L., Fuerst, F., et al. 2013, *ApJL*, 775, L45, doi: [10.1088/2041-8205/775/2/L45](https://doi.org/10.1088/2041-8205/775/2/L45)
- Miller, J. M., Gendreau, K., Ludlam, R. M., et al. 2018, *ApJL*, 860, L28, doi: [10.3847/2041-8213/aacc61](https://doi.org/10.3847/2041-8213/aacc61)
- Miniutti, G., Fabian, A. C., Goyder, R., & Lasenby, A. N. 2003, *MNRAS*, 344, L22, doi: [10.1046/j.1365-8711.2003.06988.x](https://doi.org/10.1046/j.1365-8711.2003.06988.x)
- Miniutti, G., Panessa, F., de Rosa, A., et al. 2009a, *MNRAS*, 398, 255, doi: [10.1111/j.1365-2966.2009.15092.x](https://doi.org/10.1111/j.1365-2966.2009.15092.x)
- Miniutti, G., Ponti, G., Greene, J. E., et al. 2009b, *MNRAS*, 394, 443, doi: [10.1111/j.1365-2966.2008.14334.x](https://doi.org/10.1111/j.1365-2966.2008.14334.x)
- Page, K. L., Schartel, N., Turner, M. J. L., & O'Brien, P. T. 2004, *MNRAS*, 352, 523, doi: [10.1111/j.1365-2966.2004.07939.x](https://doi.org/10.1111/j.1365-2966.2004.07939.x)
- Parker, M. L., Tomsick, J. A., Miller, J. M., et al. 2015, *ApJ*, 808, 9, doi: [10.1088/0004-637X/808/1/9](https://doi.org/10.1088/0004-637X/808/1/9)
- Petrucci, P.-O., Ursini, F., De Rosa, A., et al. 2018, *A&A*, 611, A59, doi: [10.1051/0004-6361/201731580](https://doi.org/10.1051/0004-6361/201731580)
- Petrucci, P.-O., Paltani, S., Malzac, J., et al. 2013, *A&A*, 549, A73, doi: [10.1051/0004-6361/201219956](https://doi.org/10.1051/0004-6361/201219956)
- Porquet, D., Reeves, J. N., O'Brien, P., & Brinkmann, W. 2004, *A&A*, 422, 85, doi: [10.1051/0004-6361:20047108](https://doi.org/10.1051/0004-6361:20047108)
- Pounds, K. A., Warwick, R. S., Culhane, J. L., & de Korte, P. a. J. 1986, *MNRAS*, 218, 685, doi: [10.1093/mnras/218.4.685](https://doi.org/10.1093/mnras/218.4.685)
- Reynolds, C. S., Brenneman, L. W., Lohfink, A. M., et al. 2012, *ApJ*, 755, 88, doi: [10.1088/0004-637X/755/2/88](https://doi.org/10.1088/0004-637X/755/2/88)
- Ricci, C., Tazaki, F., Ueda, Y., et al. 2014, *ApJ*, 795, 147, doi: [10.1088/0004-637X/795/2/147](https://doi.org/10.1088/0004-637X/795/2/147)
- Risaliti, G., Harrison, F. A., Madsen, K. K., et al. 2013, *Nature*, 494, 449, doi: [10.1038/nature11938](https://doi.org/10.1038/nature11938)
- Schmoll, S., Miller, J. M., Volonteri, M., et al. 2009, *ApJ*, 703, 2171, doi: [10.1088/0004-637X/703/2/2171](https://doi.org/10.1088/0004-637X/703/2/2171)
- Singh, K. P., Garmire, G. P., & Nousek, J. 1985, *ApJ*, 297, 633, doi: [10.1086/163560](https://doi.org/10.1086/163560)
- Sun, S., Guainazzi, M., Ni, Q., et al. 2018, *MNRAS*, 478, 1900, doi: [10.1093/mnras/sty1233](https://doi.org/10.1093/mnras/sty1233)
- Svoboda, J., Dovčiak, M., Goosmann, R. W., et al. 2012, *A&A*, 545, A106, doi: [10.1051/0004-6361/201219701](https://doi.org/10.1051/0004-6361/201219701)
- Tan, Y., Wang, J. X., Shu, X. W., & Zhou, Y. 2012, *ApJL*, 747, L11, doi: [10.1088/2041-8205/747/1/L11](https://doi.org/10.1088/2041-8205/747/1/L11)
- Taylor, C., & Reynolds, C. S. 2018, *ApJ*, 855, 120, doi: [10.3847/1538-4357/aaad63](https://doi.org/10.3847/1538-4357/aaad63)
- Turner, T. J., & Pounds, K. A. 1988, *MNRAS*, 232, 463, doi: [10.1093/mnras/232.2.463](https://doi.org/10.1093/mnras/232.2.463)
- Ursini, F., Dovčiak, M., Zhang, W., et al. 2020, *A&A*, 644, A132, doi: [10.1051/0004-6361/202039158](https://doi.org/10.1051/0004-6361/202039158)
- Verner, D. A., & Yakovlev, D. G. 1995, *Astronomy Astrophysics Supplement Series*, 109, 125
- Walter, R., & Fink, H. H. 1993, *A&A*, 274, 105
- Wilkins, D. R., & Fabian, A. C. 2012, *MNRAS*, 424, 1284, doi: [10.1111/j.1365-2966.2012.21308.x](https://doi.org/10.1111/j.1365-2966.2012.21308.x)
- Wilkins, D. R., García, J. A., Dauser, T., & Fabian, A. C. 2020, *MNRAS*, 498, 3302, doi: [10.1093/mnras/staa2566](https://doi.org/10.1093/mnras/staa2566)
- Xu, Y., Harrison, F. A., García, J. A., et al. 2018a, *ApJL*, 852, L34, doi: [10.3847/2041-8213/aaa4b2](https://doi.org/10.3847/2041-8213/aaa4b2)
- Xu, Y., Harrison, F. A., Kennea, J. A., et al. 2018b, *ApJ*, 865, 18, doi: [10.3847/1538-4357/aada03](https://doi.org/10.3847/1538-4357/aada03)
- Zhang, W., Dovčiak, M., & Bursa, M. 2019, *ApJ*, 875, 148, doi: [10.3847/1538-4357/ab1261](https://doi.org/10.3847/1538-4357/ab1261)